Electron Transfer from Tetrakis(isocyanide)rhodium(I) Monomers, and the Oligomers to Iron(III) and Cobalt(III) Complexes. Enhancement of the Reactivity by the Oligomerization

Shunichi Fukuzumi, Nobuaki Nishizawa, and Toshio Tanaka*

Department of Applied Chemistry, Faculty of Engineering, Osaka University, Suita, Osaka 565

(Received April 17, 1982)

Electron transfer reactions from tetrakis(isocyanide)rhodium(I) ($[RhL_4]^+$ to iron(III) complexes of the $[Fe(N\text{–}N)_3]^{3+}$ type (N–N=1,10-phenanthroline, 2,2′-bipyridine) proceed through precursor complexes formed between $[RhL_4]^+$ and $[Fe(N\text{–}N)_3]^{3+}$ with 1:1, 1:2, and 2:1 stoichiometry. A similar scheme is suggested for the reaction of bis(isocyanide)bis(triphenylphosphine)rhodium(I) with the same oxidants. The intramolecular electron transfer rate constants k_1 in the 1:1 precursor complexes have been determined in MeCN at 298 K. In accordance with Marcus theory, the log k_1 values are linearly related with the reduction potentials of oxidants with the theoretical slope of 8.5. The $[RhL_4]^+$ cations form oligomers in MeCN; $[RhL_4^+]_n$ (n=2,3), and the equilibrium constants for oligomerization have been determined. For a given oxidant $[Co(bpy)_3]^{3+}$ (bpy= 2,2′-bipyridine), the log k_1 value of $[RhL_4^+]_n$ increases in parallel with the HOMO energy of $[RhL_4^+]_n$; monomer<dimer<trimer.

Considerable interest exists in transition metal complex oligomers from the view point of their potential role in solar energy storage reaction,[1] as well as the understanding of the fundamental nature associated with the metal-metal interaction.[2] The redox properties of such metal complex oligomers, however, have scarcely been known especially in the comparison between the oligomers and the monomer. Thus, there has been no report yet on electron transfer reactions of rhodium(I) complex monomers and the oligomers, although extensive studies have been carried out on the oxidative addition reactions to rhodium(I) complexes, as well as the catalytic reactions.[3,4]

In the present study, we report kinetics of electron transfer reactions of tetrakis(isocyanide)rhodium(I) and the oligomers, $[RhL_4^+]_n$ (n=1—3) with some oxidants, $[Fe(N\text{–}N)_3]^{3+}$ (N–N=2,2′-bipyridine, substituted 1,10-phenanthrolines) and $[Co(bpy)_3]^{3+}$ (bpy=2,2′-bipyridine), as well as the effects of the ligand (L) on the oligomerization of $[RhL_4]^+$. Mechanisms for the electron transfer reactions of $[RhL_4^+]_n$ which forms highly associative precursor complexes with oxidants prior to electron transfer are discussed based on the kinetics. The intramolecular electron transfer rate constants in the precursor complexes have been obtained for both the $[RhL_4]^+$ monomers and the oligomers, and are compared in the context of the Marcus theory.[5]

Results and Discussion

Oligomerization of $[RhL_4]^+$. The $[Rh(PhNC)_4]^+$ cation has been reported to oligomerize in MeCN, yielding the dimer, $[Rh_2(PhNC)_8]^{2+}$, and the trimer, $[Rh_3(PhNC)_{12}]^{3+}$, which involve face to face contact of the $[Rh(PhNC)_4]^+$ units with weak, but direct Rh(I)–Rh(I) bonds.[2e] The formation of oligomers is characterized from the electronic spectra which show absorption bands in longer wavelengths than those due to the monomer.[2e] The electronic transition energies of the monomers, the dimers, and the trimers of a series of $[RhL_4]^+$ were determined as listed in Table 1. The equilibrium constants K_D and K_T for oligomerization defined by Eqs. 1 and 2 were determined by Eqs. 3 and 4, respectively,[2e]

$$2[RhL_4]^+ \overset{K_D}{\rightleftharpoons} [Rh_2L_8]^{2+} \quad (1)$$

$$[Rh_2L_8]^{2+} + [RhL_4]^+ \overset{K_T}{\rightleftharpoons} [Rh_3L_{12}]^{3+} \quad (2)$$

$$[Rh]/A_D^{1/2} = 1/(\varepsilon_D K_D)^{1/2} + 2A_D^{1/2}/\varepsilon_D \quad (3)$$

$$A_T = (\varepsilon_T K_T A_D^{3/2})/(\varepsilon_D^{3/2} K_D^{1/2}), \quad (4)$$

where [Rh] is the total Rh concentration in terms of the monomer, A_D and A_T are the absorbances due to dimers and trimers, respectively, and ε_D and ε_T are the corresponding molar extinction coefficients. According to Eq. 3, there is a linear relation between $[Rh]/A_D^{1/2}$ and $A_D^{1/2}$; the values of ε_D and K_T are obtained from the slope and the intercept, respectively. The K_T value is evaluated from a proportional relation between A_T and $A_D^{3/2}$ in Eq. 4, using the values of ε_D and K_D obtained from Eq. 3 as well as ε_T evaluated from the relation ε_T=1.5 ε_D.[2e] Application of Eqs. 3 and 4 to $[Rh(p\text{-}MeOC_6H_4NC)_4]^+$ and $[Rh(p\text{-}MeC_6H_4NC)_4]^+$ in MeCN containing 0.1 mol dm^{-3} n-Bu_4NClO_4 at 298 K is shown in Figs. 1a and 1b, respectively. The K_D and K_T values also are listed in Table 1. Plots of Eqs. 3 and 4 require the presence of a large amount of the oligomers within limited solubilities of $[RhL_4]^+$. Thus, when the K_D and K_T values are small (<2 mol^{-1} dm^3), Eqs. 5 and 6 are

$$A_D = \varepsilon_D K_D [Rh]^2 \quad (5)$$

$$A_T = \varepsilon_T K_D K_T [Rh]^3 \quad (6)$$

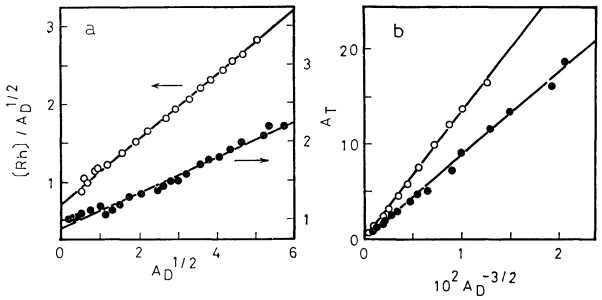

Fig. 1. Plots for the determination of (a) K_D and (b) K_T in MeCN containing 0.1 mol dm^{-3} n-Bu_4NClO_4 at 298 K; ○ $[Rh(p\text{-}MeOC_6H_4NC)_4]^+$, A_D at 564 nm and A_T at 710 nm, ● $[Rh(p\text{-}MeC_6H_4NC)_4]^+$, A_T at 563 nm and A_T at 705 nm. See Eqs. 3 and 4 in text.

used instead of Eqs. 3 and 4, respectively. By using the relations, $\varepsilon_D=2\,\varepsilon_M$ and $\varepsilon_T=3\,\varepsilon_M$,[2e] the K_D or K_T value for $[Rh(PhCH_2NC)_4]^+$ was estimated from the slope in Fig. 2a or 2b. Similarly, the K_D values for $[Rh(2,4,6\text{-}Me_3C_6H_2NC)_4]^+$ (Fig. 2a), $[Rh(t\text{-}BuNC)_4]^+$, and $[Rh(cyclo\text{-}C_6H_{11}NC)_4]^+$ were obtained from the plots of Eq. 5. No appreciable oligomer formation was observed for $[Rh(p\text{-}ClC_6H_4NC)_4]^+$, $[Rh(2,6\text{-}Me_2C_6H_3NC)_4]^+$, $[Rh(p\text{-}MeOC_6H_4NC)_2(PPh_3)_2]^+$, and $[Rh(2,4,6\text{-}Me_3C_6H_2NC)_2(PPh_3)_2]^+$.

For tetrakis(*p*-substituted phenyl isocyanide)rhodium(I), $[Rh(p\text{-}RC_6H_4NC)_4]^+$, the K_D and K_T values increase in the order R=Cl<H<Me<MeO, which is compatible with the donor ability of the para-substituents. In addition, the rhodium(I) complexes with *t*-BuNC and *cyclo*-$C_6H_{11}NC$ as ligands (Nos. 9 and 10), whose donor ability is less than PhNC,[6] oligomerize in less extents than $[Rh(PhNC)_4]^+$. On the other hand, methyl substitution on the 2,6 positions of PhNC (Nos. 5 and 6) causes substantial decrease of the K_D and K_T values compared with the corresponding rhodium(I) complexes without substituents at these positions (Nos. 2 and 3). Such a steric effect on the 2,6 positions is consistent with a staggered configration of the ligands in the crystal structure of dimeric $[Rh(PhNC)_4^+]_2$.[2e] No appreciable oligomerization in MeCN was observed also in the rhodium(I) complexes with bulky triphenylphosphine (Nos. 7 and 8). Thus, the K_D and K_T values seem to be determined by the balance between the electronic and the steric effects of the ligands.

Kinetics and Reaction Scheme for Electron Transfer Reactions between $[RhL_4]^+$ *and* $[Fe(N\text{–}N)_3]^{3+}$. Upon mixing $[Rh(p\text{-}MeC_6H_4NC)_4]^+$ and $[Fe(phen)_3]^{3+}$ in MeCN containing 0.1 mol dm^{-3} *n*-Bu_4NClO_4 at 298 K, an intense absorption band due to the reduced iron(II) species, $[Fe(phen)_3]^{2+}$, appears at 507 nm without delay. The stoichiometry of the reaction has been established as 1:1 by the spectral titration of the iron(II) species using $[Fe(phen)_3]^{2+}$ prepared independently as a reference, as shown in Fig. 3. All the rhodium(I) complexes studied here also were readily oxidized by various iron(III) complexes, $[Fe(N\text{–}N)_3]^{3+}$, as oxidants in MeCN (Eq. 7). The oxidized rhodium-

$$[RhL_4]^+ + [Fe(N\text{-}N)_3]^{3+} \longrightarrow [RhL_4]^{2+} + [Fe(N\text{-}N)_3]^{2+} \quad (7)$$

(II) species has well been regarded as radicals,[7] and dimerizes rapidly as shown in Eq. 8.[8] Thus, electron

$$2[RhL_4]^{2+} \xrightarrow{\text{fast}} [Rh_2L_8]^{4+} \quad (8)$$

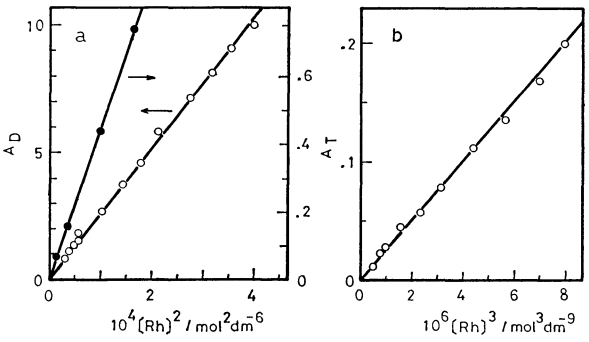

Fig. 2. Plots of (a) A_D *vs.* $[Rh]^2$ and (b) A_T *vs.* $[Rh]^3$; ● $[Rh(2,4,6\text{-}Me_3C_6H_2NC)_4]^+$, A_D at 526 nm, ○ $[Rh(PhCH_2NC)_4]^+$, A_D at 530 nm and A_T at 670 nm.

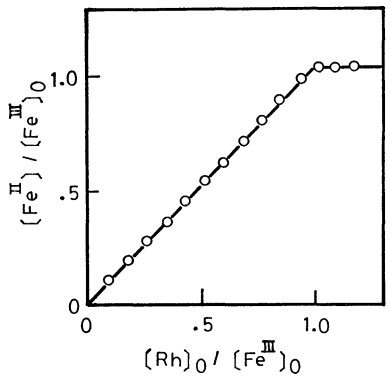

Fig. 3. Stoichiometry of the reaction between $[Rh(p\text{-}MeC_6H_4NC)_4]^+$ and $[Fe(phen)_3]^{3+}$ (1.06×10^{-4} mol dm^{-3}) in MeCN.

Table 1. Electronic transition energies of $[RhL_4^+]_n$ (n=1—3) and the equilibrium constants for the oligomer formation[a]

No.	$[RhL_4]^+$	Monomer[b]	Dimer		Trimer	
		$h\nu_M$ / eV	$h\nu_D$ / eV	K_D / mol^{-1} dm^3	$h\nu_T$ / eV	K_T / mol^{-1} dm^3
1	$[Rh(p\text{-}MeOC_6H_4NC)_4]^+$	3.08	2.20	4.3×10^2	1.75	1.3×10^2
2	$[Rh(p\text{-}MeC_6H_4NC)_4]^+$	3.05	2.20		1.76	6.2×10
3[c]	$[Rh(PhNC)_4]^+$	3.02	2.18		1.71	1.0×10
4	$[Rh(p\text{-}ClC_6H_4NC)_4]^+$	3.00	d)		d)	
5	$[Rh(2,6\text{-}Me_2C_6H_3NC)_4]^+$	3.03	d)		d)	
6	$[Rh(2,4,6\text{-}Me_3C_6H_2NC)_4]^+$	3.06	2.36	4.2×10^{-1}	d)	
7	$[Rh(p\text{-}MeOC_6H_4NC)_2(PPh_3)_2]^+$	2.97	d)		d)	
8	$[Rh(2,4,6\text{-}Me_3C_6H_2NC)_2(PPh_3)_2]^+$	3.02	d)		d)	
9	$[Rh(t\text{-}BuNC)_4]^+$	3.24	2.43	2.2×10^{-2}	d)	
10	$[Rh(cyclo\text{-}C_6H_{11}NC)_4]^+$	3.22	2.39	1.5	d)	
11	$[Rh(PhCH_2NC)_4]^+$	3.20	2.34	1.2	1.85	7.5×10^{-1}

a) In MeCN with 0.1 mol dm^{-3} *n*-Bu_4NClO_4. b) The $^1A_{1g}\rightarrow{}^1A_{2u}$ transition. c) From Ref. 2e. d) Not observed.

transfer from $[RhL_4]^+$ to $[Fe(N\text{–}N)_3]^{3+}$ is irreversible and no back electron transfer may occur.

Rates of the electron transfer reactions between $[RhL_4]^+$ and $[Fe(N\text{–}N)_3]^{3+}$ were followed by monitoring the rise of the absorbance due to $[Fe(N\text{–}N)_3]^{2+}$ in MeCN at 298 K, using a stopped flow spectrophotometer. The ionic strength was maintained constant with n-Bu_4NClO_4 (0.1 mol dm^{-3} in most cases). The reactions of $[Rh(2,4,6\text{-}Me_3C_6H_2NC)_4]^+$ and $[Rh(t\text{-}BuNC)_4]^+$ which do not oligomerize appreciably obeyed pseudo-first-order kinetics with excess amounts of either $[Fe(N\text{–}N)_3]^{3+}$ or $[RhL_4]^+$; the kinetic plots were linear over several half-lives. As typical examples, the dependences of the pseudo-first-order rate constants k_{Fe} and k_{Rh} on the concentrations of $[Fe(N\text{–}N)_3]^{3+}$ and $[Rh(2,4,6\text{-}Me_3C_6H_2NC)_4]^+$, respectively, are shown in Fig. 4. The rate constants k_{Fe} and k_{Rh} are different from each other at the same concentrations of reactants used in a large excess. In additon, k_{Rh} exhibits "saturation kinetics" with increasing the concentration of $[Rh(2,4,6\text{-}Me_3C_6H_2NC)_4]^+$, while k_{Fe} is linear against the concentration of $[Fe(N\text{–}N)_3]^{3+}$. However, the intercepts of k_{Fe} and k_{Rh} on extrapolation to [Fe]=0 and [Rh]=0, respectively, are identical, irrespective of the reactant used in excess and the ionic strength (μ=0.1 and 0.05) (Fig. 4). Such a complicated kinetics is quite different from other electron transfer reactions of transition metal complexes which show simple second-order kinetics (first-order on each reactant).[9] Furthermore, the intercept and the curveture found in Fig. 4 cannot be attributed to the reversibility of Eq. 7 in competition with the reaction in Eq. 8 since the electron transfer reaction proceeds to completion and the pseudo-first-order kinetics holds precisely under the experimental conditions in Fig. 4.

The pseudo-first-order kinetics and the complicated kinetic behavior of the pseudo-first-order rate constants in Fig. 4 may be best interpreted by assuming the following scheme for the electron transfer reaction (Eq. 7) as the rate-determining step,

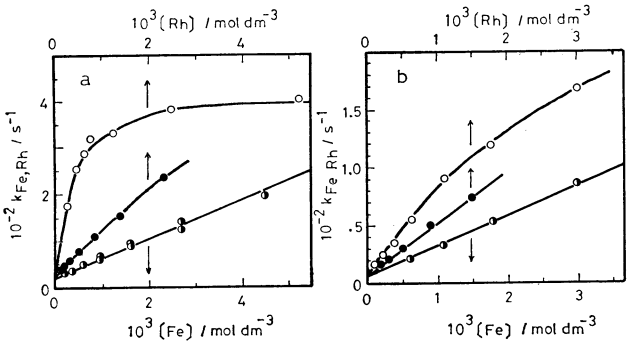

Fig. 4. Kinetics of the oxidation of $[RhL_4]^+$ (L=2,4,6-$Me_3C_6H_2NC$) with $[Fe(N\text{–}N)_3]^{3+}$; the pseudo-first-order rate constant as a function of large excess $[Fe(N\text{–}N)_3]^{3+}$ or $[RhL_4]^+$ in MeCN at 298 K; (a) N–N=phen, (b) N–N=bpy; ○ excess $[RhL_4]^+$ with 0.1 mol dm^{-3} n-Bu_4NClO_4, ● excess $[RhL_4]^+$ with 0.05 mol dm^{-3} n-Bu_4NClO_4, ◑ excess $[Fe(N\text{–}N)_3]^{3+}$ with 0.1 mol dm^{-3} n-Bu_4NClO_4.

$$[RhL_4]^+ + [Fe(N\text{–}N)_3]^{3+} \overset{K_1}{\rightleftharpoons} ([RhL_4]^+[Fe(N\text{–}N)_3]^{3+}) \xrightarrow[\text{e.t.}]{k_1} \quad (9)$$

$$([RhL_4]^+[Fe(N\text{–}N)_3]^{3+}) + [Fe(N\text{–}N)_3]^{3+} \overset{K_2}{\rightleftharpoons} ([RhL_4]^+2[Fe(N\text{–}N)_3]^{3+}) \xrightarrow[\text{e.t.}]{k_2} \quad (10)$$

$$([RhL_4]^+[Fe(N\text{–}N)_3]^{3+}) + [RhL_4]^+ \overset{K_3}{\rightleftharpoons} (2[RhL_4]^+[Fe(N\text{–}N)_3]^{3+}) \xrightarrow[\text{e.t.}]{k_3} \quad (11)$$

Scheme 1.

where e. t. represents the intramolecular electron transfer. Combination of Eq. 9 with Eqs. 10 and 11 gives the kinetic expressions of Eqs. 12 and 13, respectively,

$$k_{Fe} = \frac{k_1K_1[Fe] + k_2K_1K_2[Fe]^2}{1 + K_1[Fe] + K_1K_2[Fe]^2} \quad (12)$$

$$k_{Rh} = \frac{k_1K_1[Rh] + k_3K_1K_3[Rh]^2}{1 + K_1[Rh] + K_1K_3[Rh]^2} \quad (13)$$

for the oxidation of $[RhL_4]^+$ with $[Fe(N\text{–}N)_3]^{3+}$. When $K_1[Fe]$, $K_1[Rh] \gg 1$, Eqs. 12 and 13 are reduced to Eqs. 14 and 15, respectively.

$$k_{Fe} = \frac{k_1 + k_2K_2[Fe]}{1 + K_2[Fe]} \quad (14)$$

$$k_{Rh} = \frac{k_1 + k_3K_3[Rh]}{1 + K_3[Rh]} \quad (15)$$

The dependences of k_{Fe} and k_{Rh} on [Fe] and [Rh] in Fig. 4 are well reproduced by Eqs. 14 and 15, respectively, with the rate and the equilibrium constants listed in Table 2. The k_2, K_2, k_3, and K_3 in Eqs. 14 and 15 will be vanished at the intercepts of k_{Fe} and k_{Rh} (extrapolation to [Fe], [Rh]=0 in Fig. 4), which yield the same intramolecular electron transfer rate constant k_1 in Scheme 1. Such an intramolecular rate constant k_1 should be independent of the ionic strength of the media,[10] in accordance with the results in Fig. 4. On the other hand, the equilibrium constants K_1, K_2, and K_3 depended on the ionic strength of the media. At the ionic strength μ=0.1, the equilibrium constant K_1 was too high to be determined (K_1[Fe], $K_1[Rh] \gg 1$; $K_1 \gg 1 \times 10^4$ mol^{-1} dm^3), and Eqs. 14 and 15 were applied to the results in Fig. 4. When the ionic strength μ was reduced from 0.1 to 0.05, however, the k_{Fe} values decreased to reach zero with decreasing [Fe] in the lower concentrations ($>4.0 \times 10^{-4}$ mol dm^{-3}) in contrast with the results at μ=0.1 in Fig. 4. The K_1 values at μ=0.05 were determined by fitting the data to Eq. 12,[11] and also listed in Table 2. The rate and the equilibrium constants were evaluated also for the reaction of $[Rh(t\text{-}BuNC)_4]^+$ with $[Fe(phen)_3]^{3+}$ (Table 2).

The large equilibrium constants K_1, K_2, and K_3 (Table 2) indicate the exceptionally high affinity of the cationic oxidants towards the cationic reductants in MeCN. Such cation-cation interactions are supported by the salt effects on the equilibrium constants since if the ions are of the same sign, decreasing the ionic strength makes the equilibrium constants de-

TABLE 2. RATE AND EQUILIBRIUM CONSTANTS FOR THE ELECTRON TRANSFER REACTIONS BETWEEN $[RhL_4]^+$ AND $[Fe(N\text{-}N)_3]^{3+}$ IN MeCN AT 298 K[a)]

$[RhL_4]^+ + [Fe(N\text{-}N)_3]^{3+}$							
L	N-N	k_1 / s^{-1}	K_1[b)] / $mol^{-1}\,dm^3$	k_2 / s^{-1}	K_2 / $mol^{-1}\,dm^3$	k_3 / s^{-1}	K_3 / $mol^{-1}\,dm^3$
2,4,6-$Me_3C_6H_2NC$	bpy	2.7	7.8×10^3	d)		2.7×10^2	3.5×10^2
2,4,6-$Me_3C_6H_2NC$	phen	2.0×10	1.6×10^4	e)		4.6×10^2	2.2×10^3
t-BuNC	phen	4.0×10	c)	6.2×10^2	1.3×10^3	9.7×10^2	2.9×10^3

a) With 0.1 mol dm^{-3} *n*-Bu_4NClO_4 unless otherwise noted. b) With 0.05 mol dm^{-3} *n*-Bu_4NClO_4. With 0.1 mol dm^{-3} *n*-Bu_4NClO_4, $K \gg 1\times10^4$ $mol^{-1}\,dm^3$ (see text). c) Not determined. d) $k_2K_2 = 2.8\times10^4$ $mol^{-1}\,dm^3\,s^{-1}$. e) $k_2K_2 = 4.3\times10^4$ $mol^{-1}\,dm^3\,s^{-1}$.

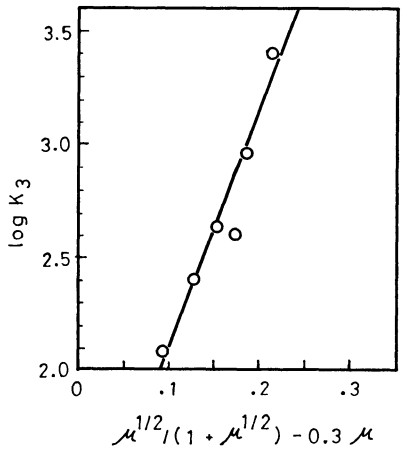

Fig. 5. Salt effect on the equilibrium constant K_3 for the oxidation of $[Rh(2,4,6\text{-}Me_3C_6H_2NC)_4]^+$ with $[Fe(phen)_3]^{3+}$; the solid line is drawn with the theoretical slope, $8A=11$ in Eq. 16, see text.[14)]

crease,[12)] as observed for K_1 (Table 2). To confirm this quantitatively, the salt effect on K_3 was examined in detail for the reaction of $[Rh(2,4,6\text{-}Me_3C_6H_2NC)_4]^+$ with $[Fe(phen)_3]^{3+}$ in MeCN at various ionic strengths adjusted by *n*-Bu_4NClO_4. The theoretical salt effect on K_3 may be given by Eq. 16 when the activity coefficients of ions are evaluated from the Davies equation,[13)]

$$\log K_3 = \log K_3^0 + 2z_Az_BA(\mu^{1/2}/(1+\mu^{1/2}) - 0.3\,\mu) \qquad (16)$$

where K_3^0 is the equilibrium constant at $\mu=0$, z_A and z_B are the charges of $([RhL_4]^+[Fe(phen)_3]^{3+})$ and $[RhL_4]^+$, respectively; $z_A=4$, $z_B=1$, and A is the Debye-Hückel coefficient.[14)] The experimental salt effect on K_3 shows reasonable agreement with the theoretical slope of Eq. 16 ($2z_Az_BA=11$) as shown in Fig. 5. Thus, Scheme 1 can account for the pseudo-first-order kinetics, the complex dependences of k_{Fe} and k_{Rh} on [Fe] and [Rh], respectively (Fig. 4), and the salt effects, which otherwise would be impossible to be explained together. The high affinity between the cationic oxidants and the cationic reductants (Table 2) is unprecedented,[15)] and at present the origin of the interaction is not clear. However, the similar affinity of $[RhL_4]^+$ towards 2,2′-bipyridine (bpy) observed in the ligand substitution reactions of $[RhL_4]^+$ with bpy[16)] suggests that the interaction between $[RhL_4]^+$ and $[Fe(N\text{-}N)_3]^{3+}$ could be mediated by the N-N ligand of $[Fe(N\text{-}N)_3]^{3+}$.

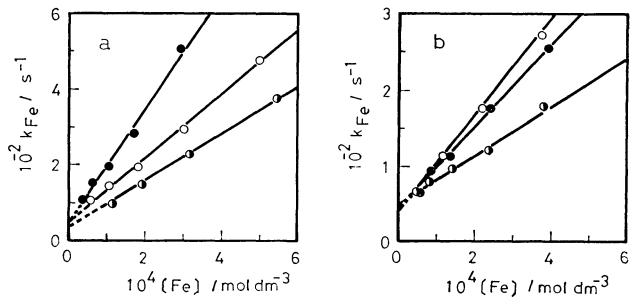

Fig. 6. Plots of the pseudo-first-order rate constant k_{Fe} for the reactions of $[RhL_4]^+$ with (a) large excess $[Fe(phen)_3]^{3+}$ and (b) $[Fe(bpy)_3]^{3+}$ in MeCN containing 0.1 mol dm^{-3} *n*-Bu_4NClO_4 at 298 K; ○ $[Rh(p\text{-}MeC_6H_4NC)_4]^+$, ● $[Rh(PhCH_2NC)_4]^+$, ◑ $[Rh(PhNC)_4]^+$.

Electron Transfer Rate Constants in the $[RhL_4]^+$ Monomer–$[Fe(N\text{-}N)_3]^{3+}$ System. Under the conditions of $K_2[Fe] \ll 1$, Eq. 14 can be reduced to Eq. 17, which predicts a linear relation between k_{Fe} and [Fe]. Plots

$$k_{Fe} = k_1 + k_2K_2[Fe] \qquad (17)$$

of the pseudo-first-order rate constant k_{Fe} against the concentrations of $[Fe(phen)_3]^{3+}$ and $[Fe(bpy)_3]^{3+}$ are illustrated in Figs. 6a and 6b, respectively. The concentrations of the Rh^I complexes used in the reactions were between 3.0×10^{-6} and 3.2×10^{-4} mol dm^{-3}, except for $[Rh(p\text{-}MeOC_6H_4NC)_4]^+$, $[Rh(p\text{-}MeC_6H_4NC)_4]^+$, and $[Rh(PhNC)_4]^+$ whose concentrations were less than 1×10^{-5} mol dm^{-3} in order to avoid the appreciable oligomerization in the higher concentrations. Under such concentrations, only monomeric $[RhL_4]^+$ may be involved in the electron transfer reactions with $[Fe(N\text{-}N)_3]^{3+}$. The electron transfer rate constants of k_1 and k_2K_2 for the $[RhL_4]^+$–$[Fe(N\text{-}N)_3]^{3+}$ system, obtained from the intercept and the slope of the plots of Eq. 17, respectively, are listed in Table 3. The k_3 and K_3 values have not been determined except for the Rh^I complexes in Table 2, because the reactions of the other Rh^I complexes in a large excess ($>1\times10^{-3}$ mol dm^{-3}) were too fast to follow by the stopped flow technique.

It is noteworthy that the k_1 value is rather independent of the ligands except for the sterically hindered 2,4,6-$Me_3C_6H_2NC$, *t*-BuNC, and PPh_3, and that the k_2K_2 value is more or less in parallel with the k_1 value. Such an insensitive dependence of k_1 as well as k_2K_2 on the diversed type ligands agrees with the

Table 3. Rate constants of electron transfer reactions between a series of rhodium(I) isocyanide complexes and $[Fe(N-N)_3]^{3+}$ in MeCN[a)]

$[RhL_4]^+$	$[Fe(bpy)_3]^{3+}$		$[Fe(phen)_3]^{3+}$	
	k_1 / s^{-1}	k_2K_2 / $mol^{-1}\,dm^3\,s^{-1}$	k_1 / s^{-1}	k_2K_2 / $mol^{-1}\,dm^3\,s^{-1}$
$[Rh(p\text{-}MeOC_6H_4NC)_4]^+$	1.2×10^2	9.0×10^4	—	—
$[Rh(p\text{-}MeC_6H_4NC)_4]^+$	3.4×10	6.5×10^5	4.6×10	8.5×10^5
$[Rh(PhNC)_4]^+$	5.0×10	3.2×10^5	3.2×10	6.1×10^5
$[Rh(p\text{-}ClC_6H_4NC)_4]^+$	5.3×10	2.1×10^5	1.5×10^2	1.7×10^5
$[Rh(2,6\text{-}Me_2C_6H_3NC)_4]^+$	8.6×10	7.4×10^5	9.4×10	5.5×10^5
$[Rh(2,4,6\text{-}Me_3C_6H_2NC)_4]^+$	2.7	2.8×10^4	2.0×10	4.3×10^5
$[Rh(p\text{-}MeOC_6H_4NC)_2(PPh_3)_2]^+$	4.0×10	2.0×10^5	4.0×10	3.5×10^5
$[Rh(2,4,6\text{-}Me_3C_6H_2NC)_2(PPh_3)_2]^+$	3.7	8.7×10^4	6.5	1.4×10^5
$[Rh(t\text{-}BuNC)_4]^+$	5.0	5.3×10^5	4.0×10	8.0×10^5
$[Rh(cyclo\text{-}C_6H_{11}NC)_4]^+$	3.7×10	3.0×10^5	7.2×10	8.1×10^5
$[Rh(PhCH_2NC)_4]^+$	4.3×10	5.4×10^5	4.6×10	1.5×10^6

a) With 0.1 mol dm^{-3} n-Bu_4NClO_4 at 298 K.

Table 4. Rate constants of electron transfer reactions between the $[RhL_4]^+$ monomer and several oxidants and reduction potentials of the oxidants[a)]

No.	Oxidants	E^0_{red} vs. SCE / V	$[Rh(t\text{-}BuNC)_4]^+$		$[Rh(2,4,6\text{-}Me_3C_6H_2NC)_4]^+$	
			k_1 / s^{-1}	k_2K_2 / $mol^{-1}\,dm^3\,s^{-1}$	k_1 / s^{-1}	k_2K_2 / $mol^{-1}\,dm^3\,s^{-1}$
1′	$[Fe(5\text{-}NO_2phen)_3]^{3+}$	1.27	3.8×10	8.1×10^4	1.1×10^2	4.0×10^4
2′	$[Fe(5\text{-}Clphen)_3]^{3+}$	1.17	3.8×10	3.8×10^5	1.3×10	2.1×10^5
3′	$[Fe(phen)_3]^{3+}$	1.07	4.0×10	3.6×10^5	2.0×10	4.3×10^4
4′	$[Fe(bpy)_3]^{3+}$	1.06	5.0	5.3×10^4	2.7	2.8×10^4
5′	$[Fe(4,7\text{-}Ph_2phen)_3]^{3+}$	1.01	3.5	7.5×10^4	4.6	1.3×10^4
6′	$[Co(bpy)_3]^{3+}$	0.31	1.5×10^{-6}	1.9×10^{-4}	1.0×10^{-6}	1.9×10^{-4}

a) In MeCN containing 0.1 mol dm^{-3} n-Bu_4NClO_4 at 298 K.

HOMO energy of the nearly nonbonding d_{z^2} level of the Rh^I complexes which may be insensitive to the difference of ligands.[17)]

Kinetic studies were performed also for the oxidation of fixed $[RhL_4]^+$ (L=t-BuNC, 2,4,6-$Me_3C_6H_2NC$) with various oxidants; $[Fe(5\text{-}NO_2phen)_3]^{3+}$, $[Fe(5\text{-}Clphen)_3]^{3+}$, $[Fe(phen)_3]^{3+}$, $[Fe(bpy)_3]^{3+}$, $[Fe(4,7\text{-}Ph_2phen)_3]^{3+}$, and $[Co(bpy)_3]^{3+}$. The electron transfer rates were measured as described above, except for the oxidation with $[Co(bpy)_3]^{3+}$ which was followed by the decay of the 440 nm and 459 nm bands of $[Rh(t\text{-}BuNC)_4]^+$ and $[Rh(2,4,6\text{-}Me_3C_6H_2NC)_4]^+$, respectively ($^1A_{1g}\rightarrow{}^3A_{2u}$ transition), in the presence of excess $[Co(bpy)_3]^{3+}$ (8.9×10^{-4}—1.0×10^{-2} mol dm^{-3}) using a conventional spectrophotometer; the reaction rate was much slower than that with $[Fe(N-N)_3]^{3+}$. The pseudo-first-order rate constant k_{Co} in the presence of excess $[Co(bpy)_3]^{3+}$ also showed a linear relation with the Co concentration. The rate constants k_1 and k_2K_2 determined from the intercept and the slope of the linear plots of k_{Fe} *vs.* [Fe] and k_{Co} *vs.* [Co] are listed in Table 4. The reduction potentials of the oxidants determined by cyclic voltammetry in MeCN also are listed in Table 4 for comparison. There can be seen a trend that the electron transfer rate constants k_1 and k_2K_2 decrease with decreasing the reduction potentials of the oxidants; this is particularly the case in $[Co(bpy)_3]^{3+}$.

Electron Transfer Rate Constants in the $[RhL_4]^+$ Oligomer–$[Co(bpy)_3]^{3+}$ System. As described in the foregoing section, high concentration solutions of $[Rh(PhNC)_4]^+$ ($>1\times10^{-3}$ mol dm^{-3}) exhibit an absorption band attributable to the dimer, $[Rh_2(PhNC)_8]^{2+}$. The rate of reaction of $[Rh(PhNC)_4]^+$ with excess $[Co(bpy)_3]^{3+}$ under such conditions was measured by monitoring the decay of an absorbance due to the dimer at 600 nm, as shown by the open circles in Fig. 7. This decay curve can be expressed by Eq. 18 as plotted by the closed circles (Fig. 7),

$$A_D^{-1/2} = at + b \qquad (18)$$

where a and b are constants as 6.4×10^{-4} s^{-1} and 1.21, respectively. On the other hand, the absorbance A_D is proportional to the square of the total amount of Rh under the experimental conditions stated in Fig. 7; A_D (at 600 nm)$=1.20\times10^5$ $[Rh]^2$. Thus, Eq. 18 may alternatively be formulated as the pseudo-second-order rate law shown in Eq. 19. It was confirmed that the decay of the absorbance due to monomeric $[Rh(PhNC)_4]^+$ at 462 nm with time also followed Eq. 19, yielding the same value of k_{Co}. Moreover, the kinetics of the oxidation of $[Rh(p\text{-}MeC_6H_4NC)_4]^+$ (4.0×10^{-4} mol dm^{-3})[18)] with $[Co(bpy)_3]^{3+}$ also followed Eq. 19, which reveals that the oxidation of the Rh^I

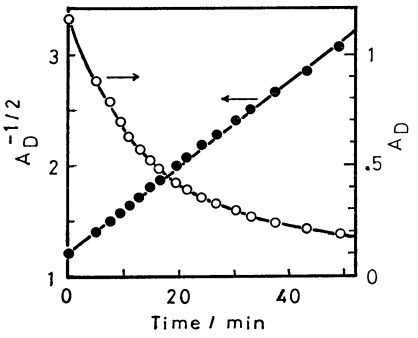

Fig. 7. Decay of the absorbance at 600 nm with time in the reaction of $[Rh_2(PhNC)_8]^{2+}$ (2.5×10^{-3} mol dm^{-3} as $[Rh(PhNC)_4]^+$) with large excess $[Co(bpy)_3]^{3+}$ (2.0×10^{-2} mol dm^{-3}) in MeCN containing 0.1 mol dm^{-3} n-Bu_4NClO_4 at 298 K (○), and the second-order plot as $A_D^{-1/2}$ *vs.* time (●), see text.

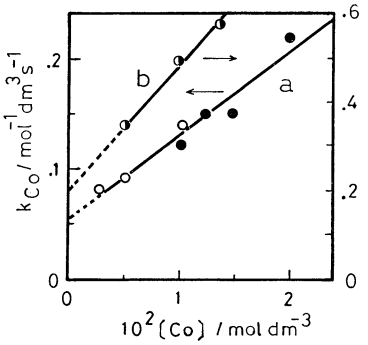

Fig. 8. Dependence of the pseudo-second-order rate constant k_{Co} on the concentration of $[Co(bpy)_3]^{3+}$ for the oxidation of (a) $[Rh(PhNC)_4]^+$ and (b) $[Rh(p\text{-}MeC_6H_4NC)_4]^+$ (4.0×10^{-4} mol dm^{-3}) in MeCN containing 0.1 mol dm^{-3} n-Bu_4NClO_4 at 298 K; ●,◑ determined from the decay of the dimer band at 600 nm, ○ determined from the decay of the monomer band at 459 nm.
The ratio of [Co]/[Rh]=10 for $[Rh(PhNC)_4]^+$.

$$-d[Rh]/dt = k_{Co}[Rh]^2 \quad (19)$$

complexes proceeds through the dimers present in solution.

The pseudo-second-order rate constants, k_{Co}/mol^{-1} dm^3 s^{-1}, obtained for the oxidation of $[Rh(PhNC)_4]^+$ and $[Rh(p\text{-}MeC_6H_4NC)_4]^+$ show linear dependences on the concentration of $[Co(bpy)_3]^{3+}$, as shown in Fig. 8. Thus, the rate constant k_{Co} is written by Eq. 20. The kinetic formulation of Eq. 20 for the dimer oxidation is analogous to that for the monomer oxidation in Eq. 17. Then, the reaction scheme for the oxidation of $[Rh(PhNC)_4]^+$ and $[Rh(p\text{-}MeC_6H_4NC)_4]^+$ with $[Co(bpy)_3]^{3+}$ may be given by combining the scheme for the monomer oxidation (Scheme 1) with the corresponding scheme for the dimer oxidation as follows.

$$k_{Co}/\text{mol}^{-1}\,\text{dm}^3\,\text{s}^{-1} = k_a + k_b[Co] \quad (20)$$

$$[RhL_4]^+ + [RhL_4]^+ \overset{K_D}{\rightleftharpoons} [Rh_2L_8]^{2+} \quad (21)$$

$$[RhL_4]^+ + [Co(bpy)_3]^{3+} \overset{K_{1M}}{\rightleftharpoons} ([RhL_4]^+[Co(bpy)_3]^{3+}) \xrightarrow[\text{e.t.}]{k_{1M}} \quad (22)$$

$$([RhL_4]^+[Co(bpy)_3]^{3+}) + [Co(bpy)_3]^{3+} \overset{K_{2M}}{\rightleftharpoons} ([RhL_4]^+2[Co(bpy)_3]^{3+} \xrightarrow[\text{e.t.}]{k_{2M}} \quad (23)$$

$$[Rh_2L_8]^{2+} + [Co(bpy)_3]^{3+} \overset{K_{1D}}{\rightleftharpoons} ([Rh_2L_8]^{2+}[Co(bpy)_3]^{3+}) \xrightarrow[\text{e.t.}]{k_{1D}} \quad (24)$$

$$([Rh_2L_8]^{2+}[Co(bpy)_3]^{3+}) + [Co(bpy)_3]^{3+} \overset{K_{2D}}{\rightleftharpoons} ([Rh_2L_8]^{2+}2[Co(bpy)_3]^{3+}) \xrightarrow[\text{e.t.}]{k_{2D}} \quad (25)$$

Scheme 2.

The second and the third steps in Scheme 2 are the same as Eqs. 9 and 10 in Scheme 1 for the monomer oxidation, respectively. The observed pseudo-second-order kinetics in excess $[Co(bpy)_3]^{3+}$ shows that the dimer oxidation (Eqs. 24 and 25) is much faster than the corresponding monomer oxidation (Eqs. 22 and 23); $k_{1D}\gg k_{1M}$, $k_{2D}\gg k_{2M}$. According to Scheme 2, the pseudo-second-order rate constant, k_{Co}/mol^{-1} dm^3 s^{-1}, is given by Eq. 26 under the conditions of $[Rh_2L_8]^{2+}\ll[RhL_4]^+$. When the equilibrium constants for the complex formation with $[Co(bpy)_3]^{3+}$ are assumed to be the same between the monomer and the dimer, *i.e.*, $K_{1D}=K_{1M}$ and $K_{2D}=K_{2M}$, Eq. 26 has an equivalent form to Eq. 12 derived from Scheme 1. Then, Eq. 26 is reduced to Eq. 27 which is analogous to Eq. 17 for the oxidation of monomeric $[RhL_4]^+$ with excess $[Fe(N\text{–}N)_3]^{3+}$. The electron transfer rate constants for the dimer, k_{1D} and $k_{2D}K_{2D}$, were thus obtained from the relations $k_a=k_{1D}K_D$ and $k_b=k_{2D}K_{2D}K_D$, respectively, using the k_a and k_b values in Eq. 20 as well as the K_D values (Table 1), and listed in Table 5. In spite of the apparant difference in the reactivity between $[Rh(PhNC)_4]^+$ and $[Rh(p\text{-}MeC_6H_4NC)_4]^+$ as seen in Fig. 8, the rate constants k_{1D} and $k_{2D}K_{2D}$ are almost the same for both dimers. This is analogous result to the oxidation of the corresponding monomers (Table 3).

$$k_{Co}/\text{mol}^{-1}\,\text{dm}^3\,\text{s}^{-1} = \frac{k_{1D}K_DK_{1D}[Co] + k_{2D}K_DK_{1D}K_{2D}[Co]^2}{1 + K_{1M}[Co] + K_{1M}K_{2M}[Co]^2} \quad (26)$$

$$k_{Co}/\text{mol}^{-1}\,\text{dm}^3\,\text{s}^{-1} = K_D(k_{1D} + k_{2D}K_{2D}[Co]) \quad (27)$$

Table 5. Electron transfer rate constants for the oxidation of $[RhL_4^+]_n$ (n=2 and 3) with $[Co(bpy)_3]^{3+}$ a)

	k_{1D} / s^{-1}	$k_{2D}K_{2D}$ / mol^{-1} dm^3 s^{-1}
$[Rh_2(PhNC)_8]^{2+}$	1.6×10^{-3}	2.2×10^{-1}
$[Rh_2(p\text{-}MeC_6H_4NC)_8]^{2+}$	1.5×10^{-3}	2.2×10^{-1}
	k_{1T}/s^{-1}	
$[Rh_3(p\text{-}MeOC_6H_4NC)_{12}]^{3+}$	5.4×10^{-1}	—

a) In MeCN with 0.1 mol dm^{-3} n-Bu_4NClO_4 at 298 K.

The kinetics of the oxidation of $[Rh(p\text{-}MeOC_6H_4NC)_4]^+$ with excess $[Co(bpy)_3]^{3+}$ was third-order in the range of the Rh concentration 1.5×10^{-4}—4.8×10^{-4} mol dm^{-3}, as expressed by Eq. 28; the third-order plots were obtained as a linear relation between A_D^{-1} *vs.* time, since $A_D=\varepsilon_D K_D[Rh]^2$. This indicates that

$$-d[Rh]/dt = k_{Co}[Rh]^3 \quad (28)$$

the oxidation occurs through trimeric $[Rh_3(p\text{-}MeOC_6H_4NC)_{12}]^{3+}$, the concentration of which is proportional to $[Rh]^3$. The pseudo-third-order rate constant k_{Co}/mol^{-2} dm^6 s^{-1} was constant irrespective of the concentration of $[Co(bpy)_3]^{3+}$ in the range of 1.4×10^{-3}—3.0×10^{-3} mol dm^{-3}, and thus k_{Co}/mol^{-2} dm^6 s^{-1}=$k_{1T}K_DK_T$. Using the K_D and K_T values in Table 1, the intramolecular electron transfer rate constant of the trimer, k_{1T}, is determined as 5.4×10^{-1} (Table 5).

Comparison of Intramolecular Electron Transfer Rate Constants between the $[RhL_4]^+$ Monomers and the Oligomers. For a particular $[RhL_4]^+$, the logarithm of the intramolecular electron transfer rate constant, $\log k_1$, varies with the reduction potentials of the oxidants (Table 4), as illustrated in Fig. 9a. Although the number of the oxidants used in this study is limited, the slope of the correlation can be expressed by Eq. 29 which is equivalent to the Marcus relation expressed by Eq. 30.[5,19]

$$\log k_1 = 8.5E^0_{red} + \text{Const} \quad (29)$$

$$\Delta G_1^* = 0.5\Delta G^0 + \text{Const} \quad (30)$$

For a given oxidant, $[Co(bpy)_3]^{3+}$, the intramolecular electron transfer rate constant k_1 of $[RhL_4^+]_n$ (n=1—3) increases in the order monomer<dimer<trimer (Tables 4 and 5). This order is in parallel with the HOMO energy level from which electron is removed; monomer<dimer<trimer, as illustrated in Fig. 10. The energy difference between the monomer and the dimer (ΔE_D) as well as the trimer (ΔE_T)

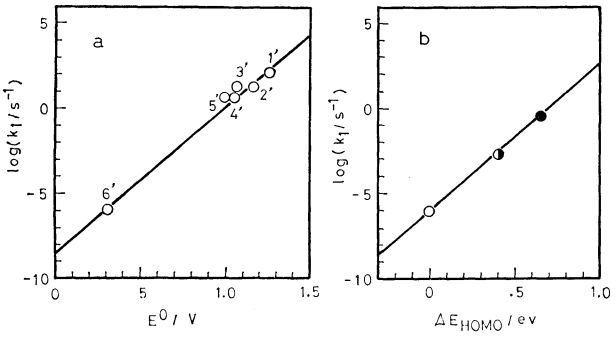

Fig. 9. Marcus plot for the intramolecular electron transfer rate constant k_1 of $[RhL_4^+]_n$ (n=1—3). (a) Plot of log k_1 for the oxidation of $[Rh(2,4,6\text{-}Me_3C_6H_2NC)_4]^+$ *vs.* the reduction potentials of the oxidants, E^0_{red}, numbers refer to the oxidants in Table 4. (b) Plot of log k_1 for the oxidation of $[RhL_4^+]_n$ with $[Co(bpy)_3]^{3+}$ *vs.* the difference in the HOMO energies, ΔE_{HOMO}, between the $[RhL_4]^+$ oligomers and the monomer; ○ $[RhL_4]^+$ (L=2,4,6-$Me_3C_6H_2NC$, *t*-BuNC), ◑ $[RhL_4^+]_2$ (L=PhNC, *p*-MeC_6H_4NC), ● $[RhL_4^+]_3$ (L=*p*-$MeOC_6H_4NC$). The lines are arbitrarily drawn with the Marcus slope of 8.5 to show the agreement,[19] see text.

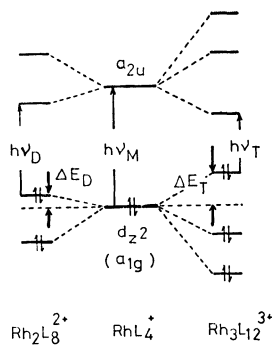

Fig.10. Energy diagram for the $[RhL_4]^+$ monomer, the dimer, and the trimer.[2e]

is estimated from the electronic transition energies listed in Table 1, using Eq. 31. A plot of log k_1 *vs.*

$$\Delta E_D = (h\nu_M - h\nu_D)/2, \quad \Delta E_T = (h\nu_M - h\nu_T)/2 \quad (31)$$

ΔE_{HOMO} thus obtained shows a linear relation as shown in Fig. 9b, from which the following equation is obtained. Thus, the Marcus slope in Eq. 29 can be

$$\log k_1 = 8.5\Delta E_{HOMO} + \text{Const} \quad (32)$$

applied also to the difference of the reactivity among the $[RhL_4]^+$ monomer, the dimer, and the trimer. The constancy of k_1 for the $[RhL_4]^+$ monomers with different ligands also accords with Eq. 32, since the HOMO energies are constant irrespective of the ligands.[17]

Summary and Conclusions. Square-planar rhodium(I) isocyanide complexes can interact with one another through the d_{z^2} HOMO orbital, yielding the dimer and the trimer. The strength of the rhodium-rhodium interaction which reflects the magnitude of the equilibrium constants for the oligomer formation is determined by the balance between electronic and steric effects of the ligands. Such availability of the interacting HOMO gives a novel feature in the electron transfer reactions. A series of $[RhL_4]^+$ forms strongly associative precursor complexes with oxidants, $[Fe(N\text{–}N)_3]^{3+}$ and $[Co(bpy)_3]^{3+}$, prior to the electron transfer. Since the oxidant or the $[RhL_4]^+$ cation can interact from both sides of the square-planar $[RhL_4]^+$, not only the 1:1 complex but also the 1:2 and the 2:1 complexes are formed between the $[RhL_4]^+$ and the oxidants. The rate constants of the intramolecular electron transfer in the precursor complexes are readily separated from the observed rate constants and largely depend on the energy difference between the HOMO of the $[RhL_4^+]_n$ (n=1—3) and the LUMO of the oxidants represented by the reduction potentials, following the Marcus relation. As such, the rate constants of intramolecular electron transfer of $[RhL_4^+]_n$ increase in the order monomer<dimer<trimer with increasing the HOMO energy.

Experimental

Materials. A series of tetrakis(isocyanide)- and bis(isocyanide)bis(triphenylphosphine)rhodium(I) perchlorates used in this study was prepared as described elsewhere.[20] 2, 2′-Bipyridine (bpy), 1,10-phenanthroline monohydrate

Table 6. Absorption spectral data for $[RhL_4^+]_n$ ($n=1$—3) in MeCN[a]

No.	$^1A_{1g}\rightarrow{}^1E_u$	$^1A_{1g}\rightarrow{}^3E_u$	$^1A_{1g}\rightarrow{}^1A_{2u}$	$^1A_{1g}\rightarrow{}^3A_{2u}$	Dimer	Trimer
1	327(25.0)	c)	403(3.15)	459(0.87)	564(4.77)	710(7.16)[e]
2	340(111)	c)	407(5.83)	462(0.85)	563(8.93)	705(13.4)[e]
3[b]	335(49.1)	c)	411(5.94)	466(0.65)	568(10.5)	c)
4	337(29.8)	c)	413(2.94)	460(0.65)	c)	c)
5	336(49.3)	c)	409(4.90)	459(0.92)	c)	c)
6	342(51.0)	c)	405(5.13)	478(0.45)	526(10.3)[d]	c)
7	345(21.9)	c)	418(3.87)	472(0.32)	c)	c)
8	330(20.5)	c)	411(4.77)	440(0.35)	c)	c)
9	309(25.3)	336(4.03)	383(10.4)	441(0.34)	510(20.8)[d]	c)
10	312(27.8)	340(3.40)	385(9.33)	443(0.40)	518(18.7)[d]	c)
11	311(35.0)	338(4.22)	387(11.0)		530(22.0)[d]	670(33.0)[e]

a) Band positions are given in nm; $\varepsilon\times10^{-3}$ values in parentheses; the number of compounds are listed in Table 1. b) Taken from Ref. 2e. c) Not observed. d) Estimated from the relation $\varepsilon_T=1.5\varepsilon_D$.

(phen), and substituted 1,10-phenanthroline (5-NO_2phen, 5-Clphen, 4,7-Ph_2phen) were obtained from Wako Pure Chemicals. The $[Fe(N\text{–}N)_3]X_2$ complexes (X=ClO_4 or PF_6; N–N=bpy, phen, 5-NO_2phen, 5-Clphen, and 4,7-Ph_2phen) were obtained according to the literature method.[21] The iron(III) complexes were synthesized as the sulfate by oxidation of the corresponding iron(II) complexes with ceric ammonium sulfate in concentrated sulfic acid. Of those, $[Fe(5\text{-}NO_2phen)_3](ClO_4)_3$ was obtained by the careful addition of 0.1 mol dm^{-3} perchloric acid to the oxidized solution, and the hexafluorophosphate salts, $[Fe(phen)_3](PF_6)_3$ and $[Fe(bpy)_3](PF_6)_3$, and the other perchlorate salts were obtained by the addition of NH_4PF_6 and $NaClO_4$, respectively. The $[Co(bpy)_3](PF_6)_3$ complex was prepared by refluxing a 30% methanol solution containing pentaamminechlorocobalt(III) chloride, $[Co(NH_3)_5Cl]Cl_2$,[22] and 2,2′-bipyridine, followed by the addition of NH_4PF_6 as described elsewhere.[23] Recrystallization was performed from hot water two times. Reagent grade acetonitrile (Wako Pure Chemicals) was purified by the standard procedure,[24] followed by redistillation from diphosphorous pentaoxide.

Oligomer Formation of $[RhL_4]^+$. Electronic absorption spectra were measured with a Union SM-401 spectrophotometer, using a 10 or 1 mm cell placed in a compartment thermostated at 298 K. Absorption maxima observed for the $[RhL_4]^+$ monomers and oligomers as well as their assignment are listed in Table 6. Equilibrium constants for the oligomer formation were determined from the change of absorbances of the $[RhL_4]^+$ oligomers as a function of the total concentration in MeCN (1×10^{-4}—1×10^{-2} mol dm^{-3}) containing 0.1 mol dm^{-3} n-Bu_4NClO_4 at 298 K. The oligomer formation of $[Rh(p\text{-}ClC_6H_4NC)_4]^+$ has not been observed in the electronic spectra because of the limited solubility in MeCN ($<2\times10^{-4}$ mol dm^{-3}). There has been found no evidence also for oligomerization of the mixed ligands rhodium(I) complexes, $[RhL_2(PPh_3)_2]^+$ (L=p-$MeOC_6H_4NC$ and 2,4,6-$Me_3C_6H_2NC$), even in nearly saturated solutions.

Electron Transfer Reactions. Acetonitrile solutions of the $[RhL_4]^+$ complexes as well as oxidants ($[Fe(N\text{–}N)_3]^{3+}$ and $[Co(bpy)_3]^{3+}$) were freshly prepared before use. The reactions were carried out at 298 K under the conditions with either the rhodium(I) complex or the oxidant in a large excess. Rates of the reactions between $[RhL_4]^+$ and $[Fe(N\text{–}N)_3]^{3+}$ were measured by monitoring the rise of absorbances due to $[Fe(N\text{–}N)_3]^{2+}$ (λ_{max}: 520 nm for $[Fe(bpy)_3]^{2+}$, 507 nm for $[Fe(phen)_3]^{2+}$, 510 nm for $[Fe(5\text{-}NO_2phen)_3]^{2+}$ and $[Fe(5\text{-}Clphen)_3]^{2+}$, and 530 nm for $[Fe(4,7\text{-}Ph_2phen)_3]^{2+}$),[25] by using a Union RA-103 stopped flow spectrophotometer. The ionic strength of the reaction medium was adjusted to 0.1 with n-Bu_4NClO_4 other than the cases to examine the effect of ionic strengths on the reaction. Rates of the reactions between $[RhL_4]^+$ and $[Co(bpy)_3]^{3+}$ were measured by monitoring the decay of the absorption band ($^1A_{1g}\rightarrow{}^3A_{2u}$) of $[RhL_4]^+$ listed in Table 6 by using a Union SM-401 spectrophotometer.

Cyclic Voltammetry. The standard reduction potentials of $[Fe(N\text{–}N)_3]^{3+}$ and $[Co(bpy)_3]^{3+}$ were measured by cyclic voltammetry on a Hokuto Denko Model HA-301 potentiostat/galvanostat. The experiments were carried out in MeCN containing 0.1 mol dm^{-3} n-Bu_4NClO_4 as a supporting electrolyte, using a platinum working electrode and a saturated NaCl calomel reference electrode. The scan rates were varied in the 20—500 mV s^{-1} range. The separation of cathodic and anodic peaks was 62 mV at the scan rate of 20 mV s^{-1} which is very close to the theoretical separation of 59 mV s^{-1} for a reversible one-electron process.[26] Attempts to measure the E^0 values for the $[RhL_4]^{+/2+}$ couple in MeCN by cyclic voltammetry have been unsuccessful; the anodic oxidation of the $[RhL_4]^+$ complexes was irreversible and no cathodic wave on the reverse scan was observed at various sweep rate between 100 and 900 mV s^{-1}.[8]

References

1) A. W. Maverick and H. B. Gray, *Pure Appl. Chem.*, **52**, 2339 (1980); H. B. Gray, K. R. Mann, N. S. Lewis, J. A. Thich, and R. M. Richma, *Adv. Chem. Ser.*, **168**, 44 (1978); I. S. Sigal, K. R. Mann, and H. B. Gray, *J. Am. Chem. Soc.*, **102**, 7252 (1980); A. W. Maverick and H. B. Gray, *ibid.*, **103**, 1298 (1981); K. R. Mann and H. B. Gray, *Adv. Chem. Ser.*, **173**, 225 (1979).

2) a) K. R. Mann, J. G. Gordon II, and H. B. Gray, *J. Am. Chem. Soc.*, **97**, 3553 (1975); b) N. S. Lewis, K. R. Mann, J. G. Gordon II, and H. B. Gray, *ibid.*, **98**, 7461 (1976); K. Kawakami, M. Haga, and T. Tanaka, *J. Organomet. Chem.*, **60**, 363 (1973); d) A. L. Balch, *J. Am. Chem. Soc.*, **98**, 8049 (1976); e) K. R. Mann, N. S. Lewis, R. M. Williams, H. B. Gray, and J. G. Gordon II, *Inorg. Chem.*, **17**, 828 (1978); f) K. Kawakami, M. Okajima, and T. Tanaka, *Bull. Chem. Soc. Jpn.*, **51**, 2327 (1978).

3) M. Haga, K. Kawakami, and T. Tanaka, *Inorg. Chim. Acta*, **12**, 93 (1975), **15**, 1946 (1976); Y. Ohtani, M. Fujimoto, and A. Yamagishi, *Bull. Chem. Soc. Jpn.*, **50**, 1453 (1977); S. Carra and R. Ugo, *Inorg. Chim. Acta Rev.*, **1**, 49 (1967); J. P. Collman and W. R. Ropper, *Adv. Organomet. Chem.*,

7, 53 (1968); A. J. Hart-Davis and W. A. G. Graham, *Inorg. Chem.*, **9**, 2658 (1970); S. Otsuka and K. Ataka, *Bull. Chem. Soc. Jpn.*, **50**, 1118 (1977); R. Kuwae, T. Tanaka, and K. Kawakami, *ibid.*, **52**, 437 (1979).

4) F. A. Cotton and G. Wilkinson, "Advanced Inorganic Chemistry," 4th ed, John Wiley & Sons Inc., New York, (1980), Chap. 30, and references cited therein.

5) R. A. Marcus, *Ann. Rev. Phys. Chem.*, **15**, 155 (1964); *J. Phys. Chem.*, **72**, 891 (1968); **67**, 853 (1963).

6) The ionization potential of alkyl isocyanide (*cyclo*-$C_6H_{11}NC$=11.0 eV, *n*-BuNC=11.1 eV) is generally higher than that of phenyl isocyanide (PhNC=9.50 eV); V. Y. Young and K. L. Cheng, *J. Elect. Spect. Relat. Phenom.*, **9**, 317 (1976).

7) T. L. Kelly and J. F. Endicott, *J. Am. Chem. Soc.*, **94**, 1797 (1972); B. B. Wayland and A. R. Newman, *ibid.*, **101**, 6472 (1979); H. Ogoshi, J. Setsune, and Z. Yoshida, *ibid.*, **99**, 3869 (1977).

8) The instability of the oxidized rhodium(II) species is shown by the cyclic voltammetry which reveals the irreversible anodic oxidation of rhodium(I) complexes; S. Fukuzumi, N. Nishizawa, and T. Tanaka, *Bull. Chem. Soc. Jpn.*, **55**, 2892 (1982).

9) M. Chou, C. Creutz, and N. Sutin, *J. Am. Chem. Soc.*, **99**, 5615 (1977); H. Taube, "Electron Transfer Reactions of Complex Ions in Solution," Academic Press, New York, (1970); W. L. Reynolds and R. W. Lummy, "Mechanisms of Electron Transfer," Ronald Press, New York, (1966).

10) J. H. Espenson, "Chemical Kinetics and Reaction Mechanisms," McGraw-Hill Inc., New York, (1981), p. 175.

11) Under the condition of $K_2[Fe] \ll 1$, Eq, 12 is reduced to the equation, $k_{Fe}=(k_1K_1[Fe]+k_2K_1K_2[Fe]^2)/(1+K_1[Fe])$, which is rewritten as the relation, $(k_{Fe}-k_2K_2[Fe])^{-1}=(k_1K_1-k_2K_2)^{-1}[Fe]^{-1}+K_1(k_1K_1-k_2K_2)^{-1}$. The equilibrium constant K_1 was determined from a linear plot of $(k_{Fe}-k_2K_2[Fe])^{-1}$ *vs.* $[Fe]^{-1}$. The k_2K_2 value was estimated from Eq. 17 for the higher concentration of Fe.

12) P. W. Atkins, "Physical Chemistry," W. H. Freeman and Comp, San Francisco, (1978), p. 914.

13) C. Davies, "Ion Association," Butterworths, London, (1962).

14) The Debye-Hückel coefficient is given by $1.825\times 10^6\ (\rho/\varepsilon^3T^3)^{1/2}$ from which A is evaluated as 1.37 in MeCN at 298 K. Then 8 A gives the slope of 11 in Fig. 5.

15) For highly charged reactants with opposite signs the interaction in the precursor complex is enhanced by the electrostatic force; A. Haim and N. Sutin, *Inorg. Chem.*, **15**, 476 (1976); A. J. Miralles, R. E. Armstrong, and A. Haim, *J. Am. Chem. Soc.*, **99**, 1416 (1977); A. P. Szecsy and A. Haim, *ibid.*, **103**, 1679 (1981); S. Kondo, Y. Sasaki, and K. Saito, *Inorg. Chem.*, **20**, 429 (1981).

16) S. Fukuzumi and T. Tanaka, unpublished data.

17) H. Isci and W. R. Mason, *Inorg. Chem.*, **14**, 913 (1975).

18) For the higher concentrations of $[Rh(p\text{-}MeOC_6H_4\text{-}NC)_4]^+$, the contribution of the trimer to the rate was not neglected.

19) Since $\Delta G^*=-2.3\,RT\log(Nhk_1/RT)$, the slope of 0.5 in Eq. 30 yields $(0.5\,F)/(2.3\,RT)=8.5$ in Eq. 29 where F is Faraday constant.

20) T. Iinuma and T. Tanaka, *Inorg. Chim. Acta*, **49**, 79 (1981).

21) M. H. Ford-Smith and N. Sutin, *J. Am. Chem. Soc.*, **83**, 1830 (1961).

22) W. A. Hyes, L. K. Yanowski, and M. Schiller, *J. Am. Chem. Soc.*, **60**, 3053 (1938).

23) P. Ellis, R. G. Wilkins, and M. T. G. Williams, *J. Chem. Soc.*, **1957**, 4456.

24) D. D. Perrin, W. L. F. Armarego, and D. R. Perrin, "Purification of Laboratory Chemicals," Pergamon Press, New York, (1966).

25) R. S. Nicholson and I. Shain, *Anal. Chem.*, **36**, 706 (1964).

26) S. Fukuzumi, C. L. Wong, and J. K. Kochi, *J. Am. Chem. Soc.*, **102**, 2298 (1980).